Enhanced optical transmission through double-layer gold slit arrays*

Xie Su-Xia(谢素霞)[a)b)], Li Hong-Jian(李宏建)[a)b)†], Zhou Xin(周 昕)[a)b)], Xu Hai-Qing(徐海清)[a)], and Fu Shao-Li(付少丽)[a)]

[a)] College of Physics Science and Technology, Central South University, Changsha 410083, China
[b)] College of Materials Science and Engineering, Central South University, Changsha 410083, China

(Received 12 June 2009; revised manuscript received 18 January 2010)

We investigate the relationship between the transmission and the layer distance of double-layer gold slit arrays by using the finite-difference time-domain method. The results show that the transmission properties can be influenced strongly by layer distance. We attribute the two types of resonant modes to surface plasmon resonance and the localised waveguide resonance. We find that the localised waveguide transmission peak redshifts and becomes broader with increasing layer distance D. We also describe and explain the splitting, shift, and degeneration of the surface plasmon resonant transmission peak theoretically. In addition, to clarify the physical mechanism of the transmission behaviours, we analyse the distributions of electric field and total energy for the three transmission peaks with distance $D = 45$ nm for the double-layer system. Light transporting behaviours are mostly concentrated in the region of the slits as well as the interspaces of the two layers, and for different resonant wavelengths the electric field and energy distributions are different. It is expected that the results obtained here will be helpful for designing subwavelength metallic grating devices.

Keywords: slit array, layer distance, localised waveguide resonance, surface plasmon resonance
PACC: 7850J, 7820P, 7320J

1. Introduction

A phenomenon known as extraordinary optical transmission, in which a thin metal film perforated with an array of subwavelength-sized slits can transmit much more light than expected, was first reported by Ebbesen *et al.* in a famous paper.[1] In this phenomenon the transmitted fraction of the incident light can exceed the open fraction of the array for certain wavelengths. The underlying mechanism for the transmission itself is intricate and merits scientific attention. Pioneering attempts to understand enhanced transmission pointed out surface plasmon polariton modes as responsible for the phenomenon. More generally, it has been shown that this behaviour occurs whenever two surface modes are coupled between themselves and weakly coupled to a continuum allowing a Fano-like description of the process.[1−3] Other explanations about the experiments of Ebbesen *et al.* have been presented, such as the localised waveguide resonances and the shape resonance dependent on the hole geometric shape, Fabry–Pérot-like guided-mode resonance of coupled-surface plasmon polarition (SPP) modes.[4,5] In an attempt to understand the underlying physical mechanisms better, many aspects of the structure have been studied including the arrangement of the subwavelength holes, the thickness of the metal film, the polarization of the incident light, the symmetry and the nonlinearity of the whole structure.[1,2,6−8] In addition, various complicated hole array structures have been proposed for even better light transmission efficiency.[9−11] The enhancement phenomenon has been widely studied partly due to the potential applications of the large transmission for one layer system.[12] Double-layer metallic subwavelength structures are investigated recently, these works focused on the effects of the lateral alignments of the slits between the two metal layers theoretically and experimentally.[13,14]

In this paper, we show transmission behaviours of a double-layer metal structure composed of two single metallic slit arrays mainly focused on the distance be-

*Project supported by the National Natural Science Foundation of China (Grant No. 60708014), the Science Foundation for Postdoctorate of China (Grant No. 2004035083), the Natural Science Foundation of Hunan Province of China (Grant No. 06JJ2034), the Excellent Doctorate Dissertation Foundation of Central South University of China (Grant No. 2008yb039) and the Hunan Provincial Innovation Foundation for Postgraduate (Grant No. CX2009B029).
†Corresponding author. E-mail: lihj398@yahoo.com.cn
© 2010 Chinese Physical Society and IOP Publishing Ltd

tween the two metal layers, assuming perfectly aligned slits. In the investigated wavelength range, we find two types of transmission resonance peaks. We attribute the two types of resonance modes to surface plasmon resonance and the localised waveguide resonance. We find that the localised waveguide transmission peak redshifts and becomes broader with increasing layer distance D. Moreover, we investigated other transmission properties, such as the increase of D, surface plasmon resonance peak's splitting, degeneration and decrease. In addition, we simulate the spatial distributions of electric field and the total energy distributions at resonance wavelength in such a kind of structures, and we describe and explain the simulation results briefly.

2. Theory

The transmission spectra and the time-dependent near fields of the metal film are numerically calculated by applying a two-dimensional finite-difference time-domain (FDTD) method. The incorporation of Maxwell equations into Yee's FDTD scheme follows instructions given in Ref. [15].

The space grid is composed of 100×700 cells in y and z directions respectively. The size of the lattice is $a \times 7a$, where $a = 750$ nm. Periodic boundary conditions are applied to the top and bottom of this unit cell. To terminate the FDTD lattice on the left and right sides of the metal films, we have employed the perfectly matched layer (PML) approach, which involves surrounding the computational cell with a medium that in theory absorbs without any reflection electromagnetic waves at all frequencies and angles of incidence. This approach is proposed by Berenger in 1994.[16] Light propagation in the metal is described by Maxwell's equations that are coupled to an equation for the light-induced oscillations of quasi-free electrons in the metal (Drude model)

$$\begin{aligned} \nabla \times \boldsymbol{E} &= -\mu_0 \frac{\partial \boldsymbol{H}}{\partial t}, \\ \nabla \times \boldsymbol{H} &= \varepsilon\varepsilon_0 \frac{\partial \boldsymbol{E}}{\partial t} + \boldsymbol{J}, \\ \frac{\partial \boldsymbol{J}}{\partial t} &+ \gamma \boldsymbol{J} = \varepsilon_0 \omega_p^2 \boldsymbol{E}, \end{aligned} \tag{1}$$

where $\boldsymbol{E}$ and $\boldsymbol{H}$ are the electric and magnetic field vectors, respectively. $\boldsymbol{J}$ is a current density (A/cm^2) corresponding to the time derivative $\boldsymbol{J} = \partial \boldsymbol{P}/\partial t$ of the metal polarization. Outside the metal film $\boldsymbol{J} \equiv 0$. The parameter ε is the relative dielectric constant, with $\varepsilon = 1$ for the air, ε_0 is the permittivity of the vacuum, $\omega_{\rm p}$ is the plasma frequency of the metal and γ is a damping rate characterizing ohmic absorption losses. Both parameters are related to the complex relative dielectric function of the metal $\varepsilon_{\rm m}$ by

$$\varepsilon_{\rm m}(\omega) = 1 - \frac{\omega_{\rm p}^2}{\omega^2 + {\rm i}\,\gamma\omega}, \tag{2}$$

where ω is the angular frequency of the incident wave, for gold, $\omega_{\rm p} = 1.374 \times 10^{16}$ s^{-1}, $\gamma = 4.08 \times 10^{13}$ s^{-1}.[17]

3. Results and discussion

Using the FDTD method, we calculate the transmissions of the double-layer gold films perforated with slits of a width $b = 132$ nm. The film is infinite in the x direction, and the thickness of each film is $h = 320$ nm; in addition, the lattice constant is $a_0 = 750$ nm. The schematic is shown in Fig. 1.

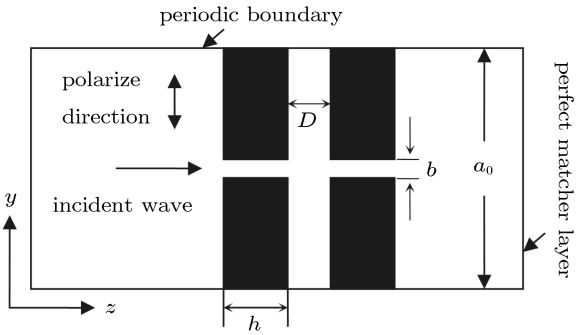


Fig. 1. Schematic illustration of the double-layer metal slit arrays structure. The $y-z$ cross section of the computational domain consisting of a single unit cell of the double-layer slit arrays. A normal incident light wave polarised along the y direction illuminates the arrays along the z direction. Periodic boundary conditions are imposed on surfaces perpendicular to the gold film, while perfect matched layers are imposed at the left and right surfaces.

A y-polarised Gaussian pulse is propagating in z direction and illuminates the metal films at normal incidence (see Fig. 1). In addition, periodic boundary conditions are imposed on the surfaces perpendicular to every gold film. Perfect matched layers are imposed at the left and right surfaces of the lattice.

As double-layer slit arrays contain two identical single-layer arrays, it is necessary to investigate the electromagnetic transmission property in single-layer array first. Single-layer array has been well investigated and the results reveal that the periodicity and thickness influence mainly the wavelength of extraordinary transmission peak, and the slit width influences mainly the amplitude and width of transmission

peak.[18−25] By changing these parameters, many interesting phenomena have been discovered and some important applications have been found.[20−22] To reveal the physical mechanisms behind the extraordinary optical transmission, here, the transmission spectra of single-layer array is investigated for different film thickness h ranging from 100 to 640 nm, to find the dependence of the wavelength of the transmission peak on the thickness h. The investigation of single-layer array could provide the useful information for understanding the enhanced transmission behaviours in double-layer slit arrays. Throughout the paper, we fix the lattice constant $a = a_0$ and the slit width $b = 132$ nm.

Figure 2 shows the normalised transmission for the single-layer gold film perforated with slits for different film thicknesses. When $h = 100$ nm, only one extraordinary transmission peak exists. When h is greater than 390 nm, the second extraordinary transmission peak appears in the shorter wavelength region near the period 750 nm, with a narrower spectral width than that of the long wavelength transmission peak. From the pictures we can find that the positions of the peaks are affected by the thickness of the gold film obviously. It is found that all peaks undergo a redshift. Moreover, we can also obtain that the resonance peak magnitude increases, and the resonance peak width becomes broader while the redshift happens. We attribute the short wavelength transmission peak to the surface plasmon resonance and the long wavelength transmission to the localised waveguide resonance. With increasing thickness of single-layer gold slit array, higher-order modes can also be supported, so more transmission peaks appear which have the very similar properties with the zeroth-order mode.

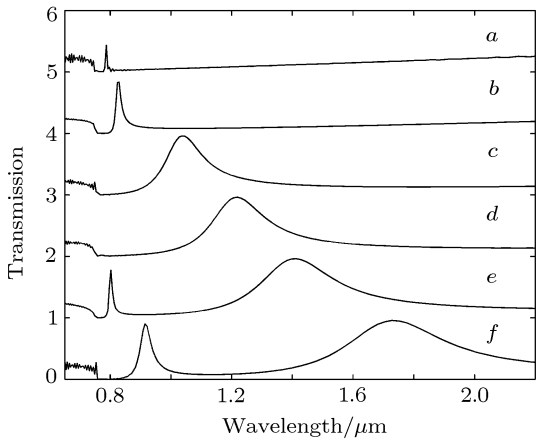


Fig. 2. Normal incident transmission of a lattice of the single-layer gold film perforated with slits with the thickness h ranging from 100 to 640 nm, curve a: $h = 100$, curve b: $h = 160$, curve c: $h = 320$, curve d: $h = 400$, curve e $h = 500$, and curve f: $h = 640$ nm.

Figure 3 shows the curve of normalised transmission versus wavelength for different layer distance D between the two metal films with thickness $h = 320$ nm. The following discussions are limited to the case of $D < 300$ nm. When D is zero, the double-layer structure can be treated as a thickened one layer gold film and the corresponding transmission spectrum shows two resonance peaks as shown in Fig. 3(a), similar to that of the one layer system. As D increases, the short wavelength transmission peak (the surface plasmon resonance) splits dramatically into two as shown in Fig. 3(b). If D increases further, the splitted resonance modes move towards each other gradually as shown in Figs. 3(c) and 3(d). When D is about 165 nm, we can find that the two splitted transmission peaks degenerate into a single one as shown in Fig. 3(e). Additionally, when D increases further more, the degenerate transmission peak does not move any more, but its magnitude becomes smaller and smaller, which may be explained by that the two single layer gold slit arrays have almost decoupled at too large D.

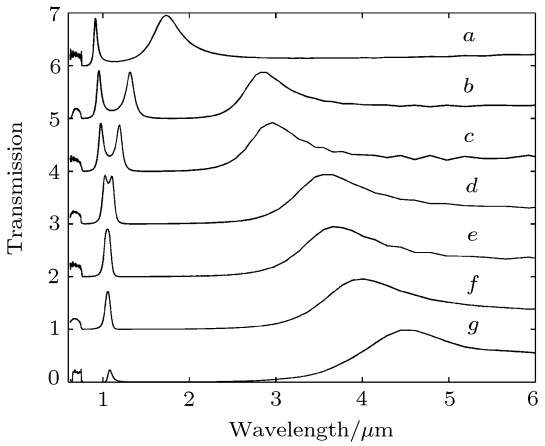


Fig. 3. Normalised transmission through the double-layer metal slit arrays for different layer spacing ranging from 0 to $0.4a$, curve a: $D = 0$, curve b: $D = 45$, curve c: $D = 75$, curve d: $D = 180$, curve e: $D = 217.5$, and curve f: $D = 300$ nm.

From Fig. 3, we can also see clearly that the transmission peak at a long wavelength (the localised waveguide resonance) has a wide band existing in all lines of these pictures. It becomes broader and broader and redshifts with increasing D. This resonance wavelength is always independent of the peri-

odicity, where each air slit can be considered as a truncated waveguide with metal walls and the two sides of it open to free space, while the truncated waveguide forms a low-Q (quality factor) cavity resonator.

From Figs. 2 and 3, what can be obtained is that the film thickness h and the layer distance D affects the transmission spectra dramatically. In the following, we present the electric field and total energy distributions of the three transmission peaks at thickness $h = 320$ nm for both films, and the layer distance $D = 45$ nm (as shown in Fig. 3(b)).

The surface plasmon polariton Bloch waves are known existing in the spatial periodic hole array in a metal film. With the normal incidence of an external excitation light, the wave vector of an excited surface plasmon Bloch wave can be written as

$$\boldsymbol{K}_{sp} = p\frac{2\pi}{L}\boldsymbol{u}_x + q\frac{2\pi}{L}\boldsymbol{u}_y, \tag{3}$$

where $\boldsymbol{u}_x$ and $\boldsymbol{u}_y$ are the unit reciprocal lattice vectors of the periodic hole array, L is its period, and p and q are integer numbers determining the surface plasmon waves propagation direction.[3] Moreover, the low-order [i.e., $(p, q) = (\pm 1, 0)$ or $(0, \pm 1)$] Bloch waves have been shown to play very important roles in the extraordinary optical transmission.[2,26] Notice that the wave vector of the excited surface plasmon Bloch waves is determined totally by the period of the hole array, as shown in Eq. (1). Due to the symmetry along the z direction, double-resonance phenomenon will appear in this structure, i.e., identical Bloch waves will be excited on the two metal–air surfaces of the metal film, and they will attenuates exponentially with increasing distance between the metal surfaces.[6] When the two layers of the gold slit arrays are placed closely, the surface plasmon Bloch waves excited in these layers couple with each other, consequently, a change of the transmission spectrum is expected.

In Figs. 4(a), 4(b), and 4(c), we can see the normal electric field $\boldsymbol{E}_y$, the tangential electric field $\boldsymbol{E}_z$ and the total energy distribution of the first transmission peak at a centre wavelength 969 nm (as shown in Fig. 3(b)). For each layer, the surface plasmon on one of the two metal–air surfaces interacts strongly with the other one which is localised on the other metal–air surface so that a 'repulsion of the levels' occurs,[27] the tangential electric field component $\boldsymbol{E}_y$ is concentrated at both ends of the slit of each layer, which can be seen in Fig. 4(a). While Fig. 4(b) shows that the normal electric field component $\boldsymbol{E}_z$ mostly localised at the metal edge of the silt, distributes along the metal film, and decays into the air. At a location inside the gap between the two layers from the output side of the first layer and the input surface of the second layer, there appear opposite charge signs, and they decouple to each other inside the air gap. As a result, the energy is found mostly localised inside the slit region in Fig. 4(c).

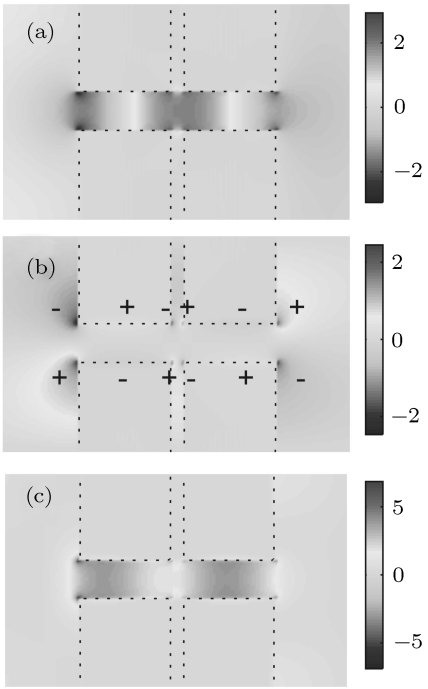


Fig. 4. The $y-z$ cross section for the amplitude evaluated at the resonant wavelength 969 nm of (a) the tangential electric field component $\boldsymbol{E}_y$, (b) the normal electric field component $\boldsymbol{E}_z$, and (c) the total energy distribution of the electromagnetic waves. The layer distance is $D = 45$ nm.

Figures 5(a), 5(b), and 5(c) show the $y - z$ cross section for the amplitude evaluated for the second transmission peak at the resonant wavelength 1323 nm (as shown in Fig. 3(b)) of the tangential electric field component $\boldsymbol{E}_y$, the normal electric field component $\boldsymbol{E}_z$, and the total energy distribution of the electromagnetic waves respectively. From Fig. 5(a) we can see that the tangential electric field component $\boldsymbol{E}_y$ is concentrated inside the slit, however it is localised at both ends of the slit in the second layer. We can find the normal electric field component $\boldsymbol{E}_z$ at the metal edge of the slit in Fig. 5(b), particularly, the strength of the normal electric field component $\boldsymbol{E}_z$ inside the gap between the two layers is much stronger. It is related to the surface charges constructively coupling. Additionally, we can see that the total energy is distributed both inside the slit and the air gap of the two

layers in Fig. 5(c).

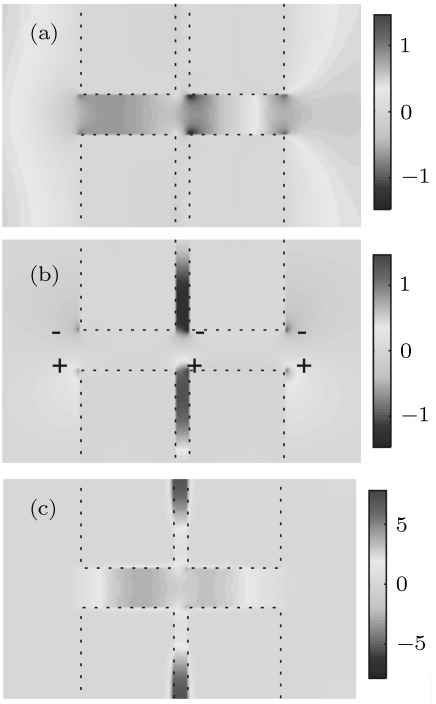


Fig. 5. The $y-z$ cross section for the amplitude evaluated at the resonant wavelength 1323 nm of (a) the tangential electric field component $\boldsymbol{E}_y$ (b), the normal electric field component $\boldsymbol{E}_z$, and (c) the total energy distribution of the electromagnetic waves. The layer distance is $D = 45$ nm.

Figures 6(a), 6(b), and 6(c) show respectively the tangential electric field $\boldsymbol{E}_y$, the normal electric field $\boldsymbol{E}_z$ and the total energy distribution of the third high transmission peak at 2826 nm (as shown in Fig. 3(b)). The normal electric field component $\boldsymbol{E}_z$ as shown in Fig. 6(b) is seen to be concentrated around the metal region along the metal edges of the first layer. It behaves as positive or negative surface charges extending to the metal region of metal–air surface between slits periodically. Such a distribution is consistent with the local charge dipole oscillation in y direction. These dipoles are flanged by opposite surface charges and these periodic charges establish a standing wave resonance in the air slit region. As a result, we can see the tangential electric field component $\boldsymbol{E}_y$ that is mostly concentrated in the slit region decaying exponentially away into air along $-z$ and z direction in Fig. 6(a). Energy transport leads to a self-guiding behaviour[28] in the gap for a localised waveguide resonance mode. The self-guiding mode will be influenced by the variation of the gap width, when the two layers are set close to each other, we can see the total energy distribution as shown in Fig. 6(c). If the gap is large enough ($D > 300$ nm), explained by the effective medium theory,[29] the double-layer system may be viewed as a multiple Fabry–Perot cavity, it will be discussed in the following works.

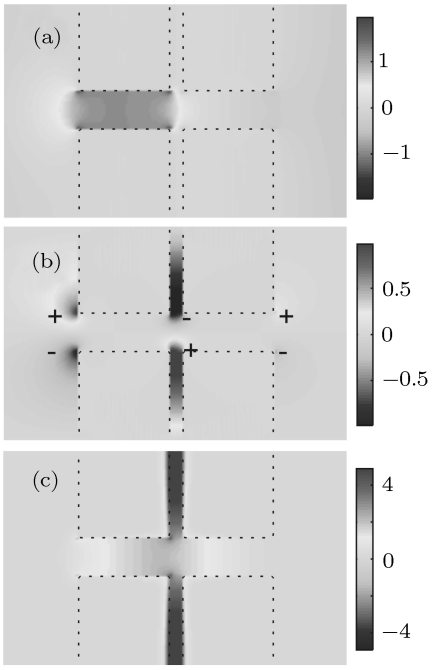


Fig. 6. The $y-z$ cross section for the amplitude evaluated at the resonant wavelength 2826 nm of (a) the tangential electric field component $\boldsymbol{E}_y$, (b) the normal electric field c component $\boldsymbol{E}_z$, and (c) the total energy distribution of the electromagnetic waves. The layer distance is $D = 45$ nm.

From Figs. 4 and 5, we can obtain that at the output surface of the first layer and the input surface of the second layer the surface plasmon modes can be supported respectively. When the two slit arrays are put close to each other, the two surface plasmon modes will couple each other. The coupled mode will propagate parallel to metal surface inside the air gap between the two layers. As a result of this coupling effect, the electromagnetic wave from the first layer can tunnel into the second one through the gap. With the decrease in layer distance D, the coupling of the surface plasmon modes becomes stronger, which results in the splitting of the transmission peak. In addition, the coupling may be associated with the diffracted evanescent waves. It has been proposed that the electromagnetic radiation propagation behaviour in the subwavelength slits can also be influenced by the interaction of evanescent wave.[30] Since the energy transports in the gap between the two films following a self-guiding behaviour, when the gap becomes larger, the resonance energy gets lower, so the centre wavelength of the localized waveguide resonance transmission peak redshifts (as shown in Fig. 3), corresponding

electric fields are shown in Fig. 6.

4. Conclusions

In conclusion, we have investigated the optical transmission properties of the double-layer gold slit arrays with changing the layer distance by using an FDTD method. Two types of resonance modes appear in the calculated spectra with increasing layer distance. It is found that the longer wavelength transmission peak redshifts and becomes broader, which is associated with the localised waveguide resonance. We also describe the peak shift, splitting and degenerating of the short wavelength resonance mode which is mostly related to the surface plasmon resonance. The corresponding electric field and total energy distributions at a certain layer distance are presented for better understanding the transmission mechanism. The results obtained in this paper may provide a useful guide to design metallic slit grating devices.

References

[1] Ebbesen T W, Lezec H J, Ghaemi H F, Thio T and Wolff P A 1998 *Nature* (London) **391** 667

[2] Martín-Moreno L, García-Vidal F J, Lezec H J, Pellerin K M, Thio T, Pendry J B and Ebbesen T W 2001 *Phys. Rev. Lett.* **86** 1114

[3] Salomon L, Grillot F D, Zayats A V and Fornel F D 2001 *Phys. Rev. Lett.* **86** 1110

[4] Ruan Z and Qiu M 2006 *Phys. Rev. Lett.* **96** 233901

[5] Cheng C, Chen J, Shi D J, Wu Q Y, Ren F F, Xu J, Fan Y X, Ding J P and Wang H T 2008 *Phys. Rev.* B **78** 075406

[6] Darmanyan S A and Zayats A V 2003 *Phys. Rev.* B **67** 035424

[7] Ren X B, Zhai T R, Ren Z, Lin J, Zhou J and Liu D H, 2009 *Acta Phys. Sin.* **58** 3208 (in Chinese)

[8] Chen X J, Wu L J, Hu W and Lan S 2009 *Acta Phys. Sin.* **58** 1025 (in Chinese)

[9] Baida F I and van Labeke D 2003 *Phys. Rev.* B **67** 155314

[10] Garcia de Abajo F J, Gomez-Santos G, Blanco L A, Borisov A G and Shabanov S V 2005 *Phys. Rev. Lett.* **95** 067403

[11] Meng T H, Zhao G Z and Zhang C L 2008 *Acta Phys. Sin.* **57** 3846 (in Chinese)

[12] Feng T H, Dai Q F, Wu L J, Guo Q, Hu W, Lan S 2008 *Chin. Phys.* B **17** 4533

[13] Marcet Z, Kwangje W, Tanner D B, Carr D W, Bower J E, Cirelli R A, Ferrt E, Klemens F, Miner J and Taylor C S 2006 *Opt. Lett.* **31** 516

[14] Marcet Z, Paster J W, Carr D W, Bower J E, Cirelli R A, Klemens F, Mansfield W M, Miner J F, Pai C S and Chan H B 2008 *Opt. Lett.* **33** 1410

[15] Yee K S 1966 *IEEE Trans. Antennas Propag.* **14** 302

[16] Berenger J P 1994 *J. Comput. Phys.* **114** 185

[17] Ordal M A, Long L L, Bell R J, Bell S E, Bell R R, Jr Alexander R W and Ward C A 1983 *Appl. Opt.* **22** 1099

[18] Zhou R L, Chen X S, Zeng Y, Zhang J B, Chen H B, Wang S W, Lu W, Li H J, Xia H and Wang L L 2008 *Acta Phys. Sin.* **57** 3506 (in Chinese)

[19] Xing Q R, Li S X, Tian Z, Liang D, Zhang N, Lang L Y, Chai L and Wang Q Y 2006 *Appl. Phys. Lett.* **89** 041107

[20] Matsui T, Agrawal A, Nahata A and Vardeny Z V 2007 *Nature* (London) **446** 517

[21] Xu T, Du C L, Wang C T and Luo X G 2007 *Appl. Phys. Lett.* **91** 201501

[22] Zhou M, Chen X S, Wang S W, Zhang J B and Lu W 2006 *Acta Phys. Sin.* **55** 3725 (in Chinese)

[23] Shi H F, Wang C T, Du C L, Luo X G, Dong X C and Gao H T 2005 *Opt. Express* **13** 6815

[24] Wang C T, Du C L and Luo X G 2006 *Phys. Rev.* B **74** 245403

[25] Hibbins A P, Hooper I R, Lockyear M J and Sambles J R 2006 *Phys. Rev. Lett.* **96** 257402

[26] Popov E, Neviere M, Enoch S and Reinisch R 2000 *Phys. Rev.* B **62** 16100

[27] Zayats A V, Smolyaninov I I and Maradudin A A 2005 *Phys. Rep.* **408** 131

[28] Li H J, Xie S X, Zhou R L, Liu Q, Zhou X and Yuan M 2008 *J. Phys.: Condens. Matter* **20** 415223

[29] Shen J T, Catrysse P B and Fan S H 2005 *Phys. Rev. Lett.* **94** 197401

[30] Hou B, Mei J, Ke M Z, Wen W J, Liu Z Y, Shi J and Sheng P 2007 *Phys. Rev.* B **76** 054303